JOURNAL OF PROPULSION AND POWER
Vol. 23, No. 2, March–April 2007

Transient Fluid Flow in Short-Pulse Operation of Bipropellant Thrusters

Brian B. Brady*
Aerospace Corporation, Los Angeles, California, 90009-2957

DOI: 10.2514/1.24611

The flow of propellants into an evacuated injector during a short pulse was measured for several propellants using two different methods. In the first method, the fluid front was observed with a high-speed camera. In the second method, the average fluid velocity during a pulse was determined from the pressure rise in the chamber from a pulse. The propellants tested were hydrazine, monomethyl hydrazine, hexane, water, and nitrogen tetroxide. The measured velocities are an order of magnitude slower than the steady-state velocities under the same conditions. The results are consistent with the development of a flow controlled by inertia and viscous drag. The implications for pulsed operation of bipropellant thrusters are discussed.

Nomenclature

A	=	area of injector
a	=	hydraulic radius
f	=	friction factor
G	=	pressure gradient
g	=	acceleration due to gravity
J_i	=	Bessel function of the first kind of order i
ℓ	=	length of injector channel
$\dot{m}$	=	propellant mass flow
P	=	pressure
Re	=	Reynolds number
r	=	radial position
t	=	time
u	=	propellant velocity in injector channel
$\bar{u}$	=	average propellant velocity in injector channel
u_{ss}	=	steady-state propellant velocity at center of injector channel
z	=	elevation
ΔP	=	pressure difference between tank and chamber
λ_n	=	nth positive root of J
μ	=	viscosity
ρ	=	density of propellant
τ	=	response time

I. Introduction

IN-SPACE propulsion is an important part of most space missions, accounting for an average of 40% of the launched mass of unmanned systems [1,2]. Pulsed bipropellant thrusters are commonly used on spacecraft for in-space propulsion. Short-pulse operation is particularly useful for attitude control, the figure of merit being the minimum impulse bit. Propellant consumption in limit-cycle operations is particularly sensitive to the minimum impulse bit [3]. A rough estimate of the size of the minimum impulse bit of a thruster is the steady-state force generated times the pulse width, but significant deviations from this concept are found experimentally [4]. Pulse widths as short as 0.01 s are used operationally. The efficiency of pulsed bipropellants has been estimated as 50% of the theoretical limit for 0.01 s pulses, rising to 75–85% for 0.1 s pulses [5]. This can be compared with a typical steady-state efficiency of 92% of theoretical. In addition to the reduced efficiency of pulsed mode operation, there is also an increased variability. The thrust can vary by ±10% from pulse to pulse, or ±30% from engine to engine [3].

Another issue affecting pulsed bipropellant thrusters is contamination. Incomplete combustion can lead to condensed phase reaction intermediates that can contaminate spacecraft surfaces [6–8] and even cause erosion [9]. These contaminants are usually seen on startup or shutdown. There is a correlation between the amount of contaminant formed and the amount the specific impulse of the pulsed mode is reduced [6,7]. In some cases, the reaction intermediates formed in incomplete combustion can lead to hard-starts or engine damage [9–11].

There are several reasons for the differences between steady-state and pulsed operation. The startup of a thruster on-orbit is significantly different from the steady-state operation. The combustion chamber is under vacuum and cold. The propellant lines from the thruster valve through the injector are also under vacuum. Just the difference in temperature is enough to cause significant differences in the flowfield [12]; the other differences compound the effect. The time required for ignition, and the establishment of steady-state combustion chamber pressure and temperature, is relatively short compared with typical thruster burns. For a short pulse meant to deliver the minimum impulse bit, however, the combustion chamber may never reach steady-state conditions within the pulse. Incomplete combustion could be one of the factors contributing to the low efficiency and high variability of pulsed thrusters, as well as the generation of contaminants. An additional potential concern is the freezing of propellant on exposure to space vacuum [13]. The purpose of this report is to study the factors that affect the delivery of propellant during short-pulse operations, and analyze the implications of these factors for the spacecraft.

II. Experiment

Experiments were conducted in a vacuum chamber. A simulated injector was created with a channel in an aluminum block with a glass cover to enable viewing of the propellant in the channel. The injector channel makes a short run from the thruster valve through the aluminum block (0.825 cm long, 0.020 cm radius), before making a 90 deg turn to run along the face of the aluminum block under the glass cover (2.90 cm long, 0.020 cm radius half cylinder). Figure 1 is a diagram of the simulated injector layout. The thruster valve was a high pressure pulsed solenoid valve. The valve was operated with a 24 V pulse from a custom-built circuit. The manufacturer lists the minimum pulse width at this voltage as 2 ms. The minimum pulse width used in these experiments was 10 ms. No fluid flow was observed for pulses less than 4 ms.

The propellants tested were monomethyl hydrazine (MMH), hydrazine, N_2O_4, water, and hexane. Water was used because it is

Received 13 April 2006; revision received 4 August 2006; accepted for publication 7 August 2006.

*Senior Scientist, Space Materials Laboratory, Mail Stop M5/754, P.O. Box 92957, Professional Member AIAA.

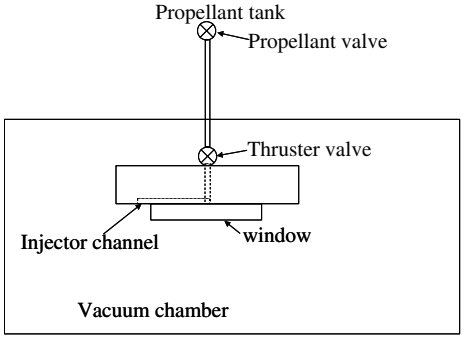

Fig. 1 Diagram of thruster valve and simulated injector channel.

nontoxic with some similar properties to the hydrazines, and it simplified the preliminary setup of the apparatus. Propellants were tested one at a time; fuel and oxidizer were never in the injector at the same time. Propellants were loaded into 1/4 in. o.d. stainless tubing behind the thruster valve. A short run of 1/8 in. o.d. tubing (~15 cm) connected the propellant reservoir to the thruster valve. This area was evacuated by opening the thruster valve to the vacuum chamber before a set of runs with a given propellant. The thruster valve was closed when the chamber base pressure was reached (~0.2 Pa), and the propellant valve was then opened allowing propellant to flow up to the thruster valve. The backing pressure was provided by a tank of nitrogen. The backing pressure was adjusted with a gas regulator. Check valves in the gas line prevented propellant vapors from entering the gas line. All runs with a given propellant were done from minimum to maximum backing pressure; this prevented the check valves from masking the apparent backing pressure. Some runs were done with the vacuum chamber vented to atmospheric pressure. The chamber was evacuated after each of these runs to remove residual propellant from the injector channel and the chamber. The chamber was evacuated with a mechanical pump (capacity ~17 ft^3/min). The vacuum plumbing connecting the mechanical pump to the chamber (the fore line) was fitted with a heated trap to scrub toxic propellant vapors from the exhaust.

Propellant velocities were measured in two different ways. In the first method, a high-speed camera was used to observe the fluid front as it progressed down the injector channel as a function of time. The fluid is visible as a dark streak in the channel, as it blocks the reflection from the back wall of the channel (see Fig. 2, which spans nine frames). Arrows indicate the position of the fluid front and the time elapsed from when fluid is first visible in the channel. The camera was run at 4500 frames per second. Knowing the total channel length allows the position of the fluid front to be calculated in each frame. The change in position as a function of time gives the velocity. This measurement gives the velocity of the fluid front only. If the fluid continues to accelerate during the pulse, that increase will not be captured in this measurement.

The second method measures the average velocity of the fluid during the pulse. In this case, the chamber is evacuated, but then the pump is isolated from the vacuum chamber by a shutoff valve before the run. The fluid injected into the vacuum chamber evaporates, and the pressure in the chamber is a measure of how much fluid was injected. The amount of propellant and the liquid density give the length of the liquid pulse. Combining the length of the liquid pulse with the pulse width in time gives the average velocity. The volume of the vacuum chamber is required to calculate the amount of fluid. In addition, the chamber pressure will not rise above the vapor pressure of the propellant, so this method works best for high vapor pressure propellants. This method was used for two propellants: hydrazine and hexane.

All experiments were conducted at temperatures between 298 and 302 K.

III. Results and Discussion

The results of the fluid velocity measuring experiments are shown in Figs. 3–7. The most surprising result is that the velocity does not

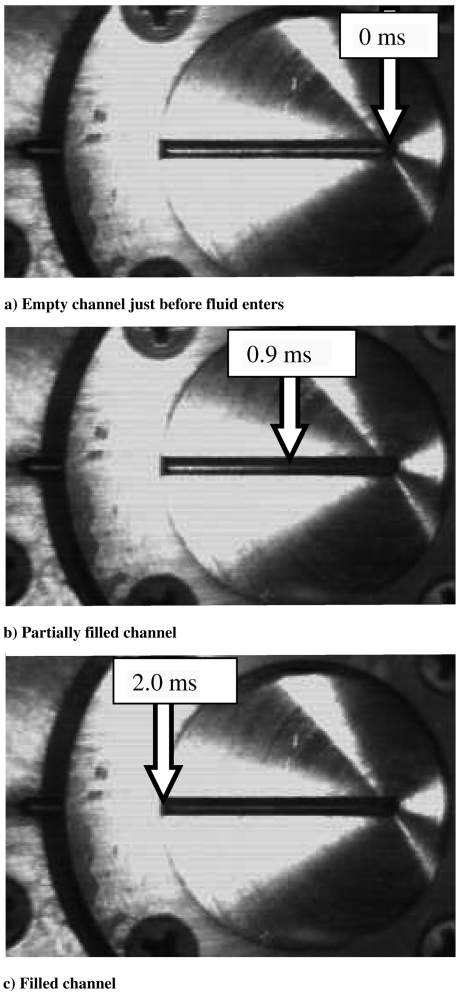

Fig. 2 Images of hexane flowing from right to left into simulated injector channel.

increase in a simple way with backing pressure. All propellants show a leveling off of velocity at fairly low values of the pressure difference (tank pressure minus chamber pressure). These velocity values are all far below the velocity calculated from the Bernoulli equation, see Eq. (1). The Bernoulli equation states that the quantity H is conserved in a flow

$$H = z + P/\rho g + u^2/2g \tag{1}$$

In the current experiments, the elevation of the propellant tank, the thruster valve, and the injector channel are all the same, so we can ignore the first term in Eq. (1). The pressure drop from the propellant tank to the chamber should then be converted to kinetic energy according to Eq. (2).

$$u = \sqrt{2\Delta P/\rho} \tag{2}$$

The observed velocity is far below this quantity, and the difference in measured velocity and calculated velocity increases with ΔP. Several possible explanations for this discrepancy are possible. One is that the energy is lost to viscous drag. We can estimate the pressure drop due to viscous drag from the equation for steady circular Poiseuille flow [14].

$$u = G\left(\frac{a^2 - r^2}{4\mu}\right) \tag{3}$$

We can rearrange this equation to solve for the pressure drop in terms of the average velocity.

$$\Delta P = \bar{u}\left(\frac{8\mu}{a^2}\right)\ell \tag{3a}$$

The assumption of steady flow is not strictly true in this case because the flow accelerates from rest. This equation overestimates the viscous pressure drop because it uses the maximum velocity over the interval. Calculating this quantity for all the propellant flow data, we find that it varies with pressure and propellant. The maximum viscous pressure drop is 7.7e4 Pa for hydrazine. The effect varies from 1–3% of the total pressure drop for all propellants at high pressures, to 25–30% at low pressures. Surprisingly, the deviation between the measured velocities and those predicted by Eq. (2) are greatest for the conditions with the least relative viscous losses.

Another way to calculate the viscous pressure drop is to add a term to the Bernoulli equation, Eq (1), representing the energy lost to friction, and incorporating an empirically derived friction factor [15]. In this formulation, the viscous pressure drop can be expressed as

$$\Delta P = \rho \bar{u}^2 f \frac{\ell}{2a} \tag{4}$$

For laminar flow, the friction factor is given by $f = 64/Re$; more complicated expressions are required for turbulent flow. Evaluating the friction factor at the transition to turbulent flow gives a value of 0.02. Using Eq. (4) to evaluate the viscous pressure drop generates higher values than Eq. (3a) with viscous drag accounting for close to 100% of the pressure drop at low pressures, but the trends are the same. The relative viscous pressure drop decreases to about 10% of the total for the large pressure drops. This approximation suffers from the same limitation as Eq. (3a) in that it assumes a steady flow. Both methods, however, indicate that the deviation of the measured velocity from the predicted value at high tank pressures cannot be explained by viscous drag.

A second explanation of the delayed flow in these experiments is that it is caused by propellant freezing. Because the chamber pressure is below the propellant vapor pressure, propellant will flash evaporate on exposure to the vacuum. The evaporation of propellant is endothermic and will absorb heat from the remaining propellant, lowering the temperature below the freezing point [13]. Freezing was observed in these experiments; frozen propellant would sometimes collect on chamber surfaces just past the end of the injector channel. Sometimes frozen drops of propellant would strike the window on the far end of the chamber. To investigate the effect of freezing we did some tests with the vacuum chamber at atmospheric pressure. With the chamber pressure above the propellant vapor pressure no flash evaporation or propellant freezing should occur. The atmospheric pressure experiments are plotted along with the vacuum chamber experiments at the appropriate ΔP in Figs. 3–7. No difference can be seen in these experiments, making it unlikely that propellant freezing plays a role in slowing the propellant flow rate.

Another explanation for the discrepancy between the measured propellant velocities and Eq. (2) is that not enough time elapses to account for the acceleration of the fluid mass.

The difference between the measured and calculated velocities can be partially explained by remembering that Eq. (2) applies to a steady-state flow. When the thruster valve is opened, the fluid velocity is zero across the channel. A flow will then begin to develop. The time it takes to reach the steady-state velocity depends on inertia and viscous drag. Bachelor [14] derives the equations governing the development of a Poiseuille flow from rest.

$$u(r,t) = \frac{G}{4\mu}(a^2 - r^2) - \frac{2Ga^2}{\mu}\sum_{n=1}^{\infty}\frac{J_0(\lambda_n r/a)}{\lambda_n^3 J_1(\lambda_n)}\exp\left(-\lambda_n^2\frac{\mu t}{\rho a^2}\right) \tag{5}$$

Figure 8 shows the development of this flow in terms of reduced velocity and reduced time. [The velocity at the center of the tube ($r = 0$) increases with time.] The reduced velocity is the velocity divided by steady-state velocity at the center of the channel. The reduced time is the time divided by the response time; see Eq. (6).

$$\tau = \rho a^2/\mu \tag{6}$$

This time dependence of the initial flow has been observed experimentally in flow in small channels [16–19]. The same response

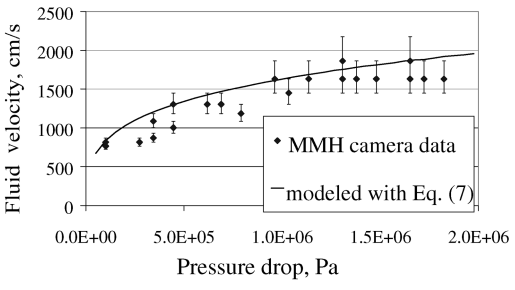

Fig. 3 MMH flow data.

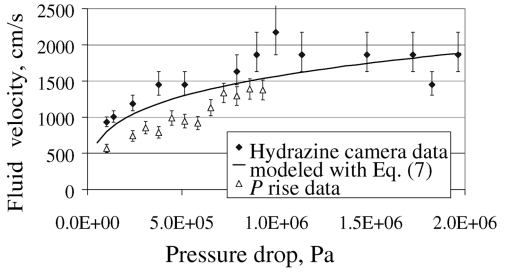

Fig. 4 Hydrazine flow data measured with two methods.

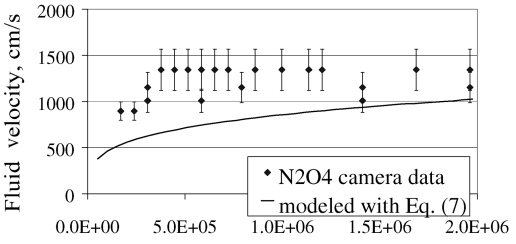

Fig. 5 N_2O_4 flow data.

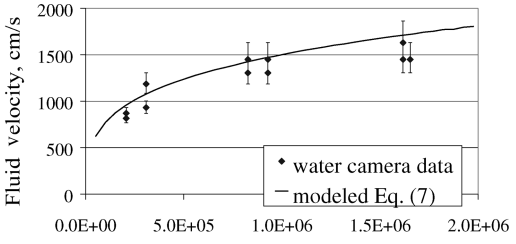

Fig. 6 Water flow data.

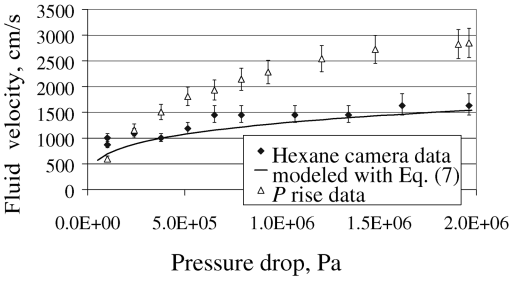

Fig. 7 Hexane flow data measured with two methods.

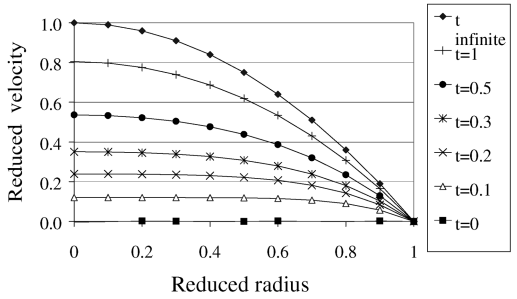

Fig. 8 Development of a laminar flow from rest. Symbols indicate radial profiles at different reduced times.

time behavior has been seen for pressure driven flows, and electroosmotic flows in cylindrical and rectangular channels.

Eq. (6) indicates that increased viscosity decreases the response time.

In the current experiment, we do not measure the radial dependence of the flow velocity. For ease of comparison with the data, therefore, we will integrate Eq. (5) over r, to obtain the average velocity over the channel cross section.

$$\bar{u}(t) = \frac{Ga^2}{8\mu}\left[1 - \sum_{n=1}^{\infty} \exp\left(-\lambda_n^2 \frac{\mu t}{\rho a^2}\right)\right] \tag{7}$$

One difficulty in evaluating this equation with respect to the current experiment is determining the value of the pressure gradient. In the experiment, the pressure is only measured at two places, in the line upstream of the thruster valve, and in the vacuum chamber at the end of the simulated injector channel. One approximation would be to assume the pressure drops linearly throughout the injector channel. For some of the flows, however, this assumption yields a kinetic energy for the flow that is greater than the energy available from the pressure drop. This probably means that the pressure drop actually occurs over a longer distance than the length of the injector channel. Instead, we will make the limiting assumption that the pressure gradient is sufficient to convert all the energy available from the pressure drop into kinetic energy.

$$G = \frac{8\mu}{a^2}\sqrt{\frac{2\Delta P}{\rho}} \tag{8}$$

Eq. (5) and Fig. 8 describe a laminar flow. The Reynolds number [Eq. (9)] is generally used to distinguish between laminar and turbulent flows. If the Re of a flow is greater than 3000, it is generally considered to be turbulent flow.

$$Re = \rho \bar{u} a/\mu \tag{9}$$

Based on the measured velocities, all of the flows in this study are turbulent. For turbulent flows, the smooth development of velocity along streamlines does not apply. The flow is not initially turbulent, as it is at rest. As the flow accelerates, vorticity is generated at the boundary. This vorticity diffuses toward the center of the channel at a rate given by the viscosity and the density [14]. The time required for the vorticity to reach the center of the channel is given by Eq. (6). This is the same as the response time. Thus, for flow times short with respect to the response time, the flow is not fully turbulent.

In Table 1, we list the response time for each propellant tested under the experimental conditions. We also list the measured time required to traverse the visible channel for the highest and lowest pressure difference. It is clear that under the conditions of the experiment, the flow has not reached steady state. The viscosity and density of the fluids are listed for reference.

If the flow is accelerating during the experiment, this might be visible in the progress of the fluid front down the injector channel. Unfortunately, the observation time is short with respect to the response time, so the expected acceleration within the observation time is small. In addition, the most reliable measurements of the velocity use the information from the entire observation time. When we make velocity measurements based on the smaller time frames, the uncertainty increases, and the scatter in the data obscures any trend in the velocity.

The pressure rise measurements should yield a higher velocity, because the flow develops during the entire 10 ms pulse. This is what is observed for hexane, (Fig. 7) but not for hydrazine (Fig. 4). Both figures show the fluid velocity measured by the high-speed camera and by the pressure rise method. The pressure rise velocities still level off at high-pressure difference for both propellants. The low vapor pressure of hydrazine did not allow the pressure rise method to be used at the higher pressure differences, where the effect of the longer acceleration time should be most noticeable. This experiment should be done with N_2O_4 and MMH, which have higher vapor pressures.

Eq. (7) can be used to model the propellant velocity as a function of the pressure difference. The velocity was calculated for a series of time steps, and the distance traveled was calculated as the sum of the velocity times the time increment. When the distance traveled equaled the length of the channel plus the distance inside the valve, the velocity at that time was plotted against the measured velocity. This procedure was repeated for each propellant. In Figs. 3–7 the calculated velocity is plotted along with the measured velocity for each of the propellants tested. The calculated velocity profile reproduces many of the features of the measured profile for each propellant. Significant deviations from the measured velocity are only seen for N_2O_4.

N_2O_4 differs from the other propellants in that it has a significant vapor pressure. The vapor pressure of N_2O_4 is near 1 atm at room temperature. It is possible that some of the N_2O_4 vaporizes in the leading edge of the pulse as it expands into a vacuum. This gas would form bubbles, lowering the density of the fluid, and allowing greater acceleration at the beginning of the pulse. This may explain why the N_2O_4 velocities are higher than predicted by Eq. (7). In addition, vapor may lead the liquid flow, and because it is dark, be mistakenly detected as liquid. Measurements using the pressure rise method would not be affected by early evaporation of the propellant or a vapor lead.

The reduced flow of propellants at short times may have some implications for thruster operation. As an example, we will examine a thruster using MMH as a fuel and N_2O_4 as the oxidizer. We will assume the thruster is designed to run steady state at a mixture ratio of 1.6. The mixture ratio is the mass flow of oxidizer divided by the mass flow of fuel; a value of 1.6 is typical [5]. Most thrusters run slightly fuel rich; the stoichiometric mixture ratio is 2.5. If both propellant tanks have the same backing pressure, the area of the oxidizer injector should be $\sim$1.25 times the area of the fuel injector to achieve the design mixture ratio. The response time, however, also depends on the area of the injector. If both the injectors have circular cross sections, the response time for the oxidizer flow will be almost

Table 1 Properties of propellants tested (densities and viscosities are at 298 K)

Propellant	Response time, s	Observed time, s		Density g/cc	Viscosity g/(s · cm)
		Low ΔP	High ΔP		
MMH	.065	.0038	.0016	0.88	7.78e − 3
Hydrazine	.066	.0031	.0016	1	8.76e − 3
N_2O_4	.197	.0071	.0020	1.43	4.2e − 3
Water	.073	.0036	.0018	1	7.98e − 3
Hexane	.127	.0033	.0018	0.6603	3.0e − 3

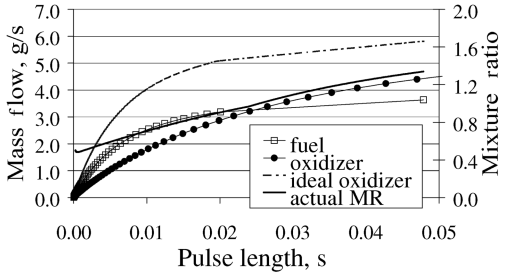

Fig. 9 Calculated propellant mass flows for a hypothetical 30 N bipropellant thruster.

four times that of the fuel. This means that for short pulses the thruster will be running very fuel rich. For a series of pulses, or a pulse train, the accumulation of excess fuel could become significant. The fuel flow, oxidizer flow, and mixture ratio as a function of pulse length are shown in Fig. 9 for this hypothetical 30 N bipropellant thruster. For the fuel $a = 0.0145$ cm, and for the oxidizer $a = 0.0163$ cm. The fluid flows were calculated by integrating Eq. (7) in time from zero to the indicated pulse length. The ideal oxidizer trace is the oxidizer flow needed for a minute ratio of 1.6 given the actual fuel flow. This analysis assumes the response time is controlled by the injector orifice, and ignores the effect of a larger diameter dribble volume.

The fact that the N_2O_4 has a faster than predicted response time in the high-speed camera experiments, Fig. 5, would seem to partially alleviate this imbalance in the mixture ratio for short pulses. If, however, the quicker response is due to propellant vaporization, and a lowering of the density as we have speculated, then the mass imbalance persists. A quicker response at a lower density still means that less mass is delivered per unit time than is necessary to oxidize the fuel stream.

The unbalanced propellant mixture in the combustion chamber exacerbates the problems associated with startup. The highly fuel rich mixture will have a lower heat release than the design mixture or a stoichiometric mixture. The smaller heat release means it will take longer to heat the chamber to operating temperature. The burning rate is also a function of temperature, which means it will take longer to release the diminished heat output. Some of the gas will exit the nozzle before optimal temperature is achieved, perhaps even before combustion is complete, generating lower thrust. The lower chamber temperature has been associated with accumulation of low vapor pressure combustion intermediates [8–11]. These intermediates may combust on subsequent pulses causing pulse-to-pulse fluctuations in the thrust output. In extreme cases, ignition of this accrued intermediate can even damage the thruster [9–11].

There is also a potential for the dynamics of the propellant line to affect steady-state operation of the thruster. The different response times of the fuel and oxidizer lines to a perturbation, such as a pressure fluctuation, may contribute to combustion instability. Because the fuel injector responds more quickly, the pressure fluctuation could cause a temporary shift in the mixture ratio that amplifies the fluctuation. The interaction between the injection dynamics, atomization, vaporization, mixing, and combustion is complex [12]. There is not enough evidence currently to test the hypothesis that unbalanced propellant injection response times can contribute to combustion instability.

Because the response time depends on the hydraulic diameter, it should be possible to design an injector with the proper mixture ratio for all pulse widths. Such a thruster would use the ratio of injector areas needed for proper steady-state operation. Instead of injectors with a single circular cross section, this thruster would use a series of holes, or a slot, or an annulus for the oxidizer to achieve the same area with a smaller hydraulic radius. Based on Eq. (7), an arrangement of four circular oxidizer injectors around a central fuel injector would have the proper mixture ratio for all pulse widths. Alternatively, a rectangular slot 10 times as long as it is wide would provide the proper response time for the oxidizer if a circular orifice were used for the fuel. This relation between the response time and the injector shape has been seen experimentally for flow in small channels [16–19], but should be verified by further experiment.

By choosing an injector with a shorter oxidizer response time, it should even be possible to run the thruster closer to a stoichiometric mixture ratio for short pulses or the beginning of longer burns, and have the thruster run at the design mixture ratio as the pulses lengthen. The higher heat release of the stoichiometric mix would bring the combustion chamber to stable operating conditions more quickly and inhibit the formation and accumulation of combustion intermediates [10,11].

The reduced flow at times shorter than the response time could be used to extend the dynamic range of the thruster. The impulse delivered by a short pulse has been estimated as the steady-state thrust times the pulse width [5]. If the propellant velocity never reaches the steady-state velocity during a pulse, however, then the impulse is reduced. If a series of pulses is used, such that the propellant mass flow rate ($\dot{m} = \bar{u}A\rho$) stays low during each pulse, then the thruster can effectively be throttled over a thrust range. The duty factor of the pulse train would reduce the average thrust even more on the low end.

Injector design involves balancing competing effects. To diminish the impact of the start transient, most injector designs try to minimize the volume of the propellant line between the thruster valve and the injector orifice, the dribble volume. This will reduce the time from the command signal to ignition and thrust. At the same time, the distance between the combustion chamber and the thruster valve needs to be large enough to prevent soak back of heat from the chamber damaging the valve; this favors a longer dribble volume. Designers also want to lessen the pressure drop from the thruster valve to the combustion chamber. This is particularly important for steady-state operation when the combustion chamber is at high pressure, and the propellants need to be at a higher pressure to be injected. This is accomplished by using a relatively large diameter for most of the dribble volume, and a thin injector orifice of smaller cross-sectional area [5]. In this way, most of the pressure drop occurs across the injector orifice. Another strategy to diminish startup effects is to force one propellant to lead the other by making its dribble volume smaller. An oxidizer lead is usually chosen; this would have the effect of moving the oxidizer curve in Fig. 9 a few milliseconds to the left, with a slight increase in the mixture ratio. Although this approach is satisfactory for steady-state operation, it can be seen from Fig. 9 that a string of short pulses will still yield a very rich mixture, with all the problems that entails.

The results from the current experiment show that a small diameter dribble volume will give the fastest response time and the shortest delay from command signal to ignition and thrust. Small diameter lines lead to large pressure drops, however, which adversely effect steady-state operation. The analysis here, however, indicates long response times are not in themselves a problem, as long as the times are similar for both propellants. As mentioned before, the reduced flow, at times short compared with the response time, may be used to provide designed low thrust levels or smaller minimum impulse bits. What is crucial is that propellants reach the combustion chamber together, allowing ignition, combustion, and high chamber temperatures and pressures. This should provide highly reproducible thrust and inhibit the accumulation of incomplete combustion products.

IV. Conclusions

In conclusion, we have investigated the transient flow properties of several propellants in a simulated injector. The results show that propellants generally do not reach steady-state velocities during the transit time for a simulated injector channel. The results are mostly consistent with a model in which the delayed response of the fluid to a pressure impulse is controlled by inertia and viscous drag. There is some discrepancy between the model and the N_2O_4 data, especially at low pressures; further tests are necessary to determine if this is due to limitations of the model or the observation method for this high vapor pressure fluid. Longer observation times relative to the response time would provide a better test of the acceleration predicted by the model. The current experiments do not test the predicted dependence of the response time on channel shape.

Acknowledgment

The author thanks Aerospace Corporation for providing support through their Independent Research and Development program.

References

[1] Sackheim, R. L., and Byers, D. C., "Status and Issues Related to In-Space Propulsion Systems," *Journal of Propulsion and Power*, Vol. 14, No. 5, 1998, pp. 669–675.

[2] Gulczinski, F. S., III, and Spores, R. A., "In-Space Propulsion," *AIAA/ICAS International Air and Space Symposium and Exposition: The Next 100Y*, AIAA Paper 2003-2588, 2003.

[3] Brown, C. D., *Spacecraft Propulsion*, AIAA, Washington, DC, 1996, Chaps. 3, 5.

[4] Gallier, P., and Pages, X., "200N Bipropellant Thruster Pulsed Mode Behavior," *35th AIAA/ASME/SAE/ASEE Joint Propulsion Conference and Exhibit*, AIAA Paper 99-2467, 1999.

[5] Sutton, G. P., *Rocket Propulsion Elements*, 6th ed., Wiley, New York, 1992, Chap. 10.

[6] Trinks, H., "Experimental Investigation of the Exhaust Plume Flow Fields of Various Small Bipropellant and Monopropellant Thrusters," *AIAA 22nd Thermophysics Conference*, AIAA Paper 87-1607, 1987.

[7] Rebrov, S., and Gerasimov, Y., "Investigation of the Contamination Properties of Bipropellant Thrusters," *35th AIAA Thermophysics Conference*, AIAA Paper 2001-2818, 2001.

[8] Woronowicz, M.S., "Alternative Description of MMH-Nitrate Formation Due to Bipropellant Thruster Operations," *38th Aerospace Sciences Meeting*, AIAA Paper 2000-0604, 2000.

[9] Takimoto, H. H., and DeNault, G. C., "Rocket Plume (N2O4/MMH) Impingement on Aluminum Surface," *Journal of Spacecraft and Rockets*, Vol. 7, No. 1, 1970, pp. 1372–1374.

[10] Mayer, S. W., Taylor, D., and Schieler, L., "Preignition Products from Propellants at Simulated High-Altitude Conditions," *Combustion Science and Technology*, Vol. 1, 1969, pp. 119–129.

[11] Juran, W., and Stechman, R. C., "Ignition Transients in Small Hypergolic Rockets," *Journal of Spacecraft and Rockets*, Vol. 5, No. 3, 1968, pp. 288–292.

[12] Pal, S., Moser, M. D., Ryan, H. M., Foust, M. J., and Santoro, R. J., "Flowfield Characteristics in a Liquid Propellant Rocket," *29th AIAA/ASME/SAE/ASEE Joint Propulsion Conference and Exhibit*, AIAA Paper 93-1882, 1993.

[13] Gayle, J. B., Egger, C. T., and Bransford, J. W., "Freezing of Liquids on Sudden Exposure to Vacuum," *Journal of Spacecraft and Rockets*, Vol. 1, No. 3, 1964, pp. 323–326.

[14] Bachelor, G. K., *Introduction to Fluid Dynamics*, Cambridge Univ. Press, Cambridge, UK, 2000, Chaps. 4–5.

[15] McKeon, B. J., Swanson, C. J., Zagarola, M. V., Donnelly, R. J., and Smits, A. J., "Friction Factors for Smooth Pipe Flow," *Journal of Fluid Mechanics*, Vol. 511, July 2004, pp. 41–44.

[16] Soderman, O., and Jonsson, B., "Electro-Osmosis: Velocity Profiles in Different Geometries with Both Temporal and Spatial Resolution," *Journal of Chemical Physics*, Vol. 105, No. 23, 1996, pp. 10,300–10,311.

[17] Yan, D., Nguyen, N., Yang, C., and Huang, X., "Visualizing the Transient Electro Osmotic Flow and Measuring the Zeta Potential of Microchannels with a Micro-Piv Technique," *Journal of Chemical Physics*, Vol. 124, No. 2, 2006, pp. 021103-1–021103-4.

[18] Yang, M. C., Ooi, K. T., Wong, T. N., and Masliyah, J. H., "Frequency-Dependent Laminar Electroosmotic Flow in a Closed-End Rectangular Microchannel," *Journal of Colloid and Interface Science*, Vol. 275, No. 2, 2004, pp. 679–698.

[19] Minor, M., van der Linde, A. J., van Leeuwen, H. P., and Lyklema, J., "Dynamic Aspects of Electrophoresis and Electroosmosis: A New Fast Method for Measuring Particle Mobilities," *Journal of Colloid and Interface Science*, Vol. 189, No. 2, 1997, pp. 370–375.

D. Talley
Associate Editor